Potential significance of photoexcited NO_2 on global air quality with the NMMB/BSC chemical transport model

O. Jorba,[1] D. Dabdub,[2] C. Blaszczak-Boxe,[3] C. Pérez,[4,5] Z. Janjic,[6] J. M. Baldasano,[1,7] M. Spada,[1] A. Badia,[1] and M. Gonçalves[1,7]

Received 5 March 2012; revised 18 May 2012; accepted 20 May 2012; published 3 July 2012.

[1] Atmospheric chemists have recently focused on the relevance of the $NO_2^* + H_2O \rightarrow OH + HONO$ reaction to local air quality. This chemistry has been considered not relevant for the troposphere from known reaction rates until nowadays. New experiments suggested a rate constant of 1.7×10^{-13} cm^3 molecule^{-1} s^{-1}, which is an order of magnitude faster than the previously estimated upper limit of 1.2×10^{-14} cm^3 molecule^{-1} s^{-1}, determined by Crowley and Carl (1997). Using the new global model, NMMB/BSC Chemical Transport Model (NMMB/BSC-CTM), simulations are presented that assess the potential significance of this chemistry on global air quality. Results show that if the NO_2^* chemistry is considered following the upper limit kinetics recommended by Crowley and Carl (1997), it produces an enhancement of ozone surface concentrations of 4–6 ppbv in rural areas and 6–15 ppbv in urban locations, reaching a maximum enhancement of 30 ppbv in eastern Asia. Moreover, NO_2 enhancements are minor (<0.01 ppbv) in background regions and reach maximum daytime values of 1–6 ppbv. Similarly, HONO exhibits negligible increases, 8–9 pptv in urban settings. Enhancements in the concentration of OH are around 14–17 $\times 10^5$ molec cm^{-3}. Decreases in the concentration of O_3 and its precursors are also identified but to a lesser degree. In order to quantify the role of the two kinetic rates measured, model simulations are compared after incorporating both reaction rate constants. Maximum O_3 difference enhancements from 5 to 10 ppbv are modeled over locations where high NO_x emissions are present; however, differences are small in most parts of the globe.

Citation: Jorba, O., D. Dabdub, C. Blaszczak-Boxe, C. Pérez, Z. Janjic, J. M. Baldasano, M. Spada, A. Badia, and M. Gonçalves (2012), Potential significance of photoexcited NO_2 on global air quality with the NMMB/BSC chemical transport model, *J. Geophys. Res.*, *117*, D13301, doi:10.1029/2012JD017730.

1. Introduction

[2] The chemistry of electronically excited NO_2 and H_2O has gained interest during the last years for its implication in the enhancement of hydroxyl radical (OH) production. It is well-known that OH radicals are the most important oxidant in the atmosphere during the day. Photolysis of O_3 in the presence of water vapor is the major source of OH radicals:

$$O_3 + h\nu(\lambda \leq 320nm) \rightarrow O_2 + O(^1D) \quad (1)$$

$$O(^1D) + H_2O \rightarrow 2OH \quad (2)$$

$$O(^1D) + M \rightarrow O(^3P) + M. \quad (3)$$

[3] In addition, other well-recognized sources of OH in the troposphere are

$$HONO + h\nu(\lambda < 390nm) \rightarrow OH + NO \quad (4)$$

$$H_2O_2 + h\nu \rightarrow 2OH \quad (5)$$

$$HO_2 + NO \rightarrow NO_2 + OH. \quad (6)$$

[1]Earth Sciences Department, Barcelona Supercomputing Center, Barcelona, Spain.
[2]Department of Mechanical and Aerospace Engineering, University of California, Irvine, California, USA.
[3]Department of Physical, Environmental and Computer Science, Medgar Evers College, City University of New York, New York, USA.
[4]NASA Goddard Institute for Space Studies, New York, New York, USA.
[5]Department of Applied Physics and Applied Math, Columbia University, New York, New York, USA.
[6]National Centers for Environmental Prediction, Camp Springs, Maryland, USA.
[7]Environmental Modeling Laboratory, Projects Department, Technical University of Catalonia, Barcelona, Spain.

Corresponding author: O. Jorba, Earth Sciences Department, Barcelona Supercomputing Center, Jordi Girona 31, Barcelona, ES-08034, Spain. (oriol.jorba@bsc.es)

©2012. American Geophysical Union. All Rights Reserved.
0148-0227/12/2012JD017730

[4] Fast gas-phase photochemical cycles involving NO_2 influence tropospheric O_3 concentrations. NO_2 absorbs sunlight strongly and is in rapid photochemical equilibrium with NO_x and O_3 [*Leighton*, 1961]:

$$NO_2 + h\nu(\lambda \leq 420nm) \rightarrow NO + O \quad (7)$$

$$O + O_2 + M \rightarrow O_3 + M \quad (8)$$

$$NO + O_3 \rightarrow NO_2 + O_2. \quad (9)$$

[5] The NO_2 absorption spectrum displays two broad continua centered at ca. 400 and 210 nm [*Crowley and Carl*, 1997]. Due to the filtering effect of O_3 in the stratosphere, only wavelengths longer than 300 nm are relevant for photochemistry in the troposphere. Under high tropospheric solar zenith angles, the UV flux is depleted, and other OH production mechanism become relevant. In this sense, when NO_2 absorbs sunlight photon between 400 and 650 nm, NO_2 photoexcites to NO_2^*. Then, the reaction of NO_2^* with H_2O can be a major source of tropospheric OH radicals [*Li et al.*, 2008]:

$$NO_2 + h\nu(\lambda > 420nm) \rightarrow NO_2^* \quad (10)$$

$$NO_2^* + M \rightarrow NO_2 + M \quad (11)$$

$$NO_2^* + H_2O \rightarrow OH + HONO. \quad (12)$$

[6] *Li et al.* [2008] reported that the bimolecular reaction of electronically excited NO_2^* with H_2O can lead to substantial OH production. Previous results from *Crowley and Carl* [1997] suggested that the photoexcitation chemistry of NO_2 producing OH radicals is not relevant in the atmosphere, suggesting an upper limit rate constant for the photoexcited NO_2^* with H_2O reaction of 1.2×10^{-14} cm^3 molecule^{-1} s^{-1}, an order of magnitude lower than that determined by *Li et al.* [2008], 1.7×10^{-13} cm^3 molecule^{-1} s^{-1}.

[7] *Crowley and Carl* [1997] and *Li et al.* [2008] add another level of complexity to the current understanding of production of ozone and its precursors. Reaction rate constants quantified by these studies, therefore, lead to enhanced production of O_3 due to the net production of OH. This is due to the comparable reaction efficiency of OH production via the $NO_2^* + H_2O$ reaction channel (e.g., 1 in 10,000 of the NO_2^* molecules produced reacts with H_2O to produce OH and HONO) compared as described in reactions (1–3) to the classical OH source (i.e., by way of ozone photolysis) and the fact that the amount of OH produced from NO_2^* scales linearly with the amount of NO_2 in the atmosphere [*Wennberg and Dabdub*, 2008]. In other words, despite the minor branching of the $NO_2 + h\nu$ reaction to produce NO_2^*, which in turn reacts with H_2O to produces OH and HONO, typical concentrations of NO_2 (30 to 100 ppbv = 7×10^{11} to 2×10^{12} molecule cm^{-3}) are much larger than that of OH (8×10^{-3} to 0.5 pptv = 2×10^5 to 1×10^7 molecule cm^{-3}).

[8] Such different reaction rate constants have led several authors to analyze the impact of this new rate coefficient on tropospheric air quality. *Wennberg and Dabdub* [2008] analyzed the impact of the new kinetics in the South Coast Air Basin of California during a typical summer episode from 1987 with the University of California, Irvine - California Institute of Technology (UCI-CIT) model. The authors used both reaction rate constants and reported an enhancement of O_3 formation by as much as 55 ppbv using the rates reported by *Li et al.* [2008]. On the other hand, *Sarwar et al.* [2009] argued that the previous results of *Wennberg and Dabdub* [2008] were limited to assess the impact of the new kinetics on contemporary emissions. Thus, *Sarwar et al.* [2009] implemented the new kinetics within CMAQ model and assessed the impact in the U.S. during July 2001 and 2002. The authors reported maximum increases of O_3 production in some urban areas of 9 ppbv in eastern U.S. and 6 ppbv in western U.S., significantly smaller than those previously reported by *Wennberg and Dabdub* [2008]. Finally, *Ensberg et al.* [2010] studied the impacts of the new chemistry on air pollution control strategies within the South Coast Air Basin of California with the UCI-CIT model. Results with past emission conditions from 1987 and current conditions from 2005 were discussed. The sensitivity of modeled pollutant control strategies due to the inclusion of the photoexcitation on NO_2 decreases with the decrease in baseline emissions from 1987 to 2005. Maximum increases in 8-h average O_3 concentrations of 8 ppbv were reported for the 2005 case. Furthermore, the authors conclude that the inclusion of the new rates increases the sensitivity of ozone concentrations with respect to changes in NO_x emissions.

[9] Additional studies have investigated the impact of reaction (12) [*Wentzell et al.*, 2010; *Li et al.*, 2011; *Sörgel et al.*, 2011]. *Wentzell et al.* [2010] modeled observed HONO values at the Harrow, Ontario, Canada supersite, via incorporating reaction (12) and could not account for the measured excess HONO produced since the calculated production rate is a factor of 2–6 larger. *Sörgel et al.* [2011] utilized the *Crowley and Carl* [1997] and *Li et al.* [2008] kinetics to model HONO measurements during the Diel Oxidant Mechanism In relation to Nitrogen Oxides (DOMINO) campaign in southwest Spain; they showed that the *Li et al.* [2008] kinetics contributed to ~8% toward HONO measurements, while using the *Crowley and Carl* [1997] kinetics exhibited negligible amounts of HONO. *Li et al.* [2011] used the WRF-Chem model to model HONO, NO_y, and O_3 observations over Beijing, Tianjin, and Hebei Provinces of China, which they note (in addition, to including updated HONO emissions, heterogeneous reactions on aerosol surfaces), considerably improve HONO and O_3 simulations in these respective regions.

[10] It has been shown that the emission regime plays an important role on the impacts of the chemistry [e.g., *Wennberg and Dabdub*, 2008; *Sarwar et al.*, 2009; *Ensberg et al.*, 2010]. From all previous results, an important question arises: What is the possible impact of photoexcited NO_2 chemistry on a global scale? In the present work, global simulations, produced from an online chemical transport model and constrained by reaction rate constants proposed by *Crowley and Carl* [1997] (as an upper limit) and *Li et al.* [2008] are analyzed for the first time to elucidate

quantitatively the impact of the NO_2^* chemistry. The impact of the photoexcited chemistry is first discussed within the context of comparing simulations with and without *Crowley and Carl* [1997] NO_2^* kinetics within a default tropospheric chemical mechanism, Carbon-Bond 05 (CB05) [*Yarwood et al.*, 2005]. Thereafter, the impact of considering *Li et al.* [2008] NO_2^* kinetics is also evaluated in comparison to both simulations, with and without *Crowley and Carl* [1997] NO_2^* kinetics.

[11] The following section discusses the uncertainties among proposed reaction rate constants for reaction (12). Section 3 describes the model and the experimental setup. The results and evaluation of the model simulations are discussed in section 4, and a final summary and conclusion section is presented in section 5.

2. Uncertainties on Reaction Rates of Photoexcited NO_2^*

[12] *Li et al.* [2008] reported a reaction rate constant of $k_{12} = 1.7 \times 10^{-13}$ cm^3 molecule^{-1} s^{-1}, which is an order magnitude greater than the upper limit proposed by *Crowley and Carl* [1997] ($k_{12} = 1.2 \times 10^{-14}$ cm^3 molecule^{-1} s^{-1}). Thereafter, *Carr et al.* [2009] argued that the NO_2^* reaction with H_2O likely does not occur under normal atmospheric conditions although they produce a reaction rate a factor of 17 lower than that reported by *Li et al.* [2008], which similar to the result of *Crowley and Carl* [1997] at the 2 σ level. Similar to *Carr et al.* [2009], *Li et al.* [2009] then responded by stating that the reason for the differences in the results of the two studies are not obvious especially when considering that the reaction under consideration is a difficult one to study due to rapid quenching of NO_2^* by water and low product yields [*Li et al.*, 2008]. *Carr et al.* [2009] and *Li et al.* [2009] both point out that the difference in experimental approach may contribute to this incongruence, specifically, the use of unfocused laser light [*Carr et al.*, 2009] compared to the use of a lens to focus the laser light [*Li et al.*, 2008]. *Li et al.* [2008] used OH from the vibrational overtone-induced unimolecular dissociation of CH_3OOH ($5v_{OH}$) to calibrate OH yields, whereas *Carr et al.* [2009] used the photodissociation of acetone, followed by the reaction of the resulting acetyl radical with O_2 for their calibrations. *Carr et al.* [2009] suggest that the differences in the results may be primarily due to multiphoton effects, contributing to the OH signal in their study, which would be sourced from the greater laser power density created by the presence of the lens. *Carr et al.* [2009] cites the presence of an intercept appearing the linear power dependence plot in *Li et al.* [2008] as indicative of multiphoton effects. *Carr et al.* [2009] did not suggest a mechanism for which OH could be produced by the multiphoton excitation process and was not able to provide data on the effect of increasing power density in their measurements of the OH yield as the maximum laser fluence used their experiments was below the threshold required by *Li et al.* [2008] to generate an OH signal. Yet *Li et al.* [2009] found no compelling evidence that multiphoton effects contributed to formation of OH radicals after investigating several multiphoton mechanism: a) multiphoton dissociation of NO_2 to produce $O(^1D)$, which can react with H_2 to produce OH radicals [*Sander et al.*, 2006]; b) the production of translationally hot ground state $O(^3P)$ atoms from the multiphoton dissociation of NO_2, which in principle can react with water to produce OH radicals; c) populating long-lived bound excited quartet electronic excited states of NO_2 through multiphoton excitation, which then reacts with H_2O to produce OH; and d) the primary source of measured OH signal were due to the collision of electronically excited NO_2 with vibrationally excited H_2O. The first scenario was ruled out as the introduction of H_2 in to the experimental cell in place of H_2O did not produce any measurable amount of OH. The second scenario was also ruled out as the $O(^3P)$ reaction is endothermic by $\sim$17 kcal mole^{-1} [*Sander et al.*, 2006], and the translational energy generated from the photodissociation of NO_2 is not sufficiently energetic to initiate the $O(^3P) + H_2O$ reaction (e.g., 0.3 eV ($\sim$6.9 kcal mole^{-1} at 308 nm)). Although NO_2 has several excited quartet states in the vicinity of 3.61 to 4.37 eV, accessing these bound excited electronic NO_2 from the ground state requires the involvement of spin-forbidden transitions. Moreover, although these bound excited states could potentially be accessed through sequential two-photon excitation by the intermediate A^2B_2 electronic state of NO_2, initially populated through the excitation in the visible range, spectral features of bound-to-bound transitions, such as these should be reflected in their characteristic structured excitation spectrum. *Li et al.* [2008] produce an action spectrum from the $NO_2^* + H_2O$ reaction that match the expected $X^2A_1 \rightarrow A^2B_2$ excitation of NO_2 in the visible range. In addition to being spin-forbidden in regards to their photochemical formation, the bimolecular reaction of bound excited state NO_2 with H_2O is also expected to be spin-forbidden. The last scenario was ruled out as *Li et al.* [2008] did not produce a squared-dependence for the pseudo first-order rates. They do note, however, that this pathway, may contribute to small background levels of OH.

[13] Recently, *Amedro et al.* [2011] contribute to this controversial reaction by way of using the coupling of a Fluorescence Assay be Gas Expansion (FAGE) instrument to a laser photolysis cell. They claim that no OH radicals were observed using an unfocused excitation laser beam at 565 nm, but OH was measured by focusing the laser beam. Based on the dependence of the OH-fluorescence signal with the laser energy, they deduce that the OH radicals are sourced from a complex mechanism that includes multiphoton absorption of NO_2. *Amedro et al.* [2011] quantify an upper-limit OH yield of 8×10^{-6} for reaction (12), which is in accordance with *Crowley and Carl* [1997] and *Carr et al.* [2009], who estimate OH-yield upper-limits of 7×10^{-5} and 6×10^{-5}, respectively. Within this context, *Crowley and Carl* [1997] also quantify a reaction rate for reaction (12) of 1.2×10^{14} cm^3 molecule^{-1} s^{-1}, which is, again, 1-order of magnitude less than that measured by *Li et al.* [2008], i.e., 1.7×10^{13} cm^3 molecule^{-1} s^{-1}.

[14] Assuming all the uncertainties around reaction (12) rate constant, in the present work, the potential significance of this chemistry is assessed at global scale applying the suggested rates of both *Li et al.* [2008] and *Crowley and Carl* [1997].

3. Methods

3.1. Numerical Model

[15] The model used for this study is the NMMB/BSC Chemical Transport Model (NMMB/BSC-CTM) [*Pérez*

Table 1. Model Configuration

Meteorology	Configuration
Dynamics	NMMB
Physics	Ferrier microphysics, BMJ cumulus scheme, MYJ PBL scheme, LISS land surface model, GFDL radiation
Chemistry	**Configuration**
Chemical mechanism	Carbond Bond 05
Photolysis scheme	Fast-J
Dry deposition	Wesely scheme
Cloud chemistry	Binkowsky scheme
Biogenic emissions	MEGAN
Resolution and Initial Conditions	**Value**
Horizontal resolution	$1.4^\circ \times 1^\circ$
Vertical layers	64
Top of the atmosphere	0 hPa
Initial condition	LMDz-INCA
Spin-up	6 month

et al., 2011; *Jorba et al.*, 2011; *Pérez et al.*, 2009; *Jorba et al.*, 2009]. It is an online chemical weather prediction system for mesoscale to global-scale applications, developed at the Barcelona Supercomputing Center. The atmospheric driver is the NCEP/NMMB multiscale numerical weather prediction model, developed at the National Centers for Environmental Prediction (NCEP). A description of the modeling system is presented in this section. Table 1 summarizes the main characteristics of the NMMB/BSC-CTM model.

3.1.1. The Atmospheric Driver: NMMB

[16] The Non-hydrostatic Multiscale Model on the B grid (NMMB) [*Janjic*, 2005; *Janjic and Black*, 2007; *Janjic et al.*, 2011] is a new unified atmospheric model for a broad range of spatial and temporal scales. Its unified non-hydrostatic dynamical core allows regional and global simulations. The regional NMMB is the operational regional North American Mesoscale (NAM) model at NCEP. The numerical schemes used in the model were designed following the principles set up in *Janjic* [1977, 1979, 1984, 2003]. Isotropic horizontal finite volume differencing is employed so a variety of basic and derived dynamical and quadratic quantities are conserved. The hybrid pressure-sigma coordinate [*Simmons and Burridge*, 1981] is used in the vertical and the Arakawa B-grid horizontal staggering is applied in the horizontal. The unified version of the model is developed for the scales ranging from large eddy simulations (LES) to global simulations [*Janjic*, 2005]. The non-hydrostatic component of the model dynamics is introduced through an add-on module that can be turned on or off, depending on resolution. The physical package used is composed by: (1) the Mellor-Yamada-Janjic (MYJ) level 2.5 turbulence closure for the treatment of turbulence in the planetary boundary layer (PBL) and in the free atmosphere [*Janjic*, 2001], (2) the surface layer scheme based on the Monin-Obukhov similarity theory [*Monin and Obukhov*, 1954] with introduced viscous sublayer over land and water [*Zilitinkevich*, 1965; *Janjic*, 1994], (3) the NCEP NOAH land surface model [*Ek et al.*, 2003] or the LISS model [*Vukovic et al.*, 2010] for the computation of the heat and moisture surface fluxes, (4) the GFDL longwave and shortwave radiation [*Fels and Schwarzkopf*, 1975; *Lacis and Hansen*, 1974], (5) the Ferrier gridscale clouds and microphysics [*Ferrier et al.*, 2002], and (6) the Betts-Miller-Janjic convective adjustment scheme [*Betts*, 1986; *Betts and Miller*, 1986; *Janjic*, 1994, 2000]. Vertical diffusion is handled by the surface layer scheme and by the PBL scheme. Lateral diffusion is formulated following the Smagorinsky non-linear approach [*Janjic*, 1990].

3.1.2. Online Gas-Phase Chemistry

[17] The gas-phase tropospheric chemistry is inlined within the NMMB code. Meteorological information is available at each time step to solve the chemical processes properly. In order to maintain full consistency with the meteorological solver, chemical species are advected and mixed at the corresponding time step of the meteorological tracers using the same numerical schemes implemented in the NMMB. The advection scheme is Eulerian, positive definite and monotone, maintaining a consistent mass-conservation of the chemical species within the domain of study [*Janjic et al.*, 2009; *Tang et al.*, 2009].

[18] For the present study, the Carbon-Bond 2005 (CB05) is used [*Yarwood et al.*, 2005]. It is an updated version of the Carbon-Bond IV (CB4) lumped-structure-type mechanism of *Gery et al.* [1989]. The CB4 mechanism was formulated focusing on limited domain extent, urban environments and for planetary boundary layer chemistry. In this sense, the CB05 extends its applicability from urban to remote tropospheric conditions and is suitable for global applications.

[19] The CB05 core mechanism has 51 chemical species and solves 156 reactions. It considers 20 photolytic reactions and extends inorganic reactions from urban to remote tropospheric conditions. The rate constants are updated based on evaluations of *Atkinson et al.* [2004] and *Sander et al.* [2006]. The organic compounds not explicitly treated are apportioned to the carbon-bond species based on the molecular structure and following *Yarwood et al.* [2005] assignments from VOC species to CB05 model species.

[20] No explicit stratospheric chemistry is implemented in the current version of the model. Stratospheric gas-phase concentrations are initialized from climatological profiles or from a global chemical model and are constant throughout a given simulation.

[21] One of the most important processes determining tropospheric composition is the photo-dissociation of trace gases. 20 photolysis reactions are considered in the standard configuration of the model. To compute the photolysis rates, the Fast-J [*Wild et al.*, 2000] online photolysis scheme is implemented. The quantum yields and cross section for the CB05 photolysis reactions have been revised and updated following the recommendations of *Atkinson et al.* [2004] and *Sander et al.* [2006].

[22] An online implementation is used to characterize the dry-deposition of atmospheric species following the *Wesely* [1989] scheme. The cloud chemistry scheme of *Byun and Ching* [1999] and *Foley et al.* [2010] has been implemented within NMMB/BSC-CTM in order to resolve the cloud processes affecting the concentration of air pollutants. The processes included are grid-scale scavenging and wet-deposition, subgrid-scale vertical mixing, scavenging and wet-deposition for precipitating and non-precipitating clouds. Only in-cloud scavenging is considered in the current implementation.

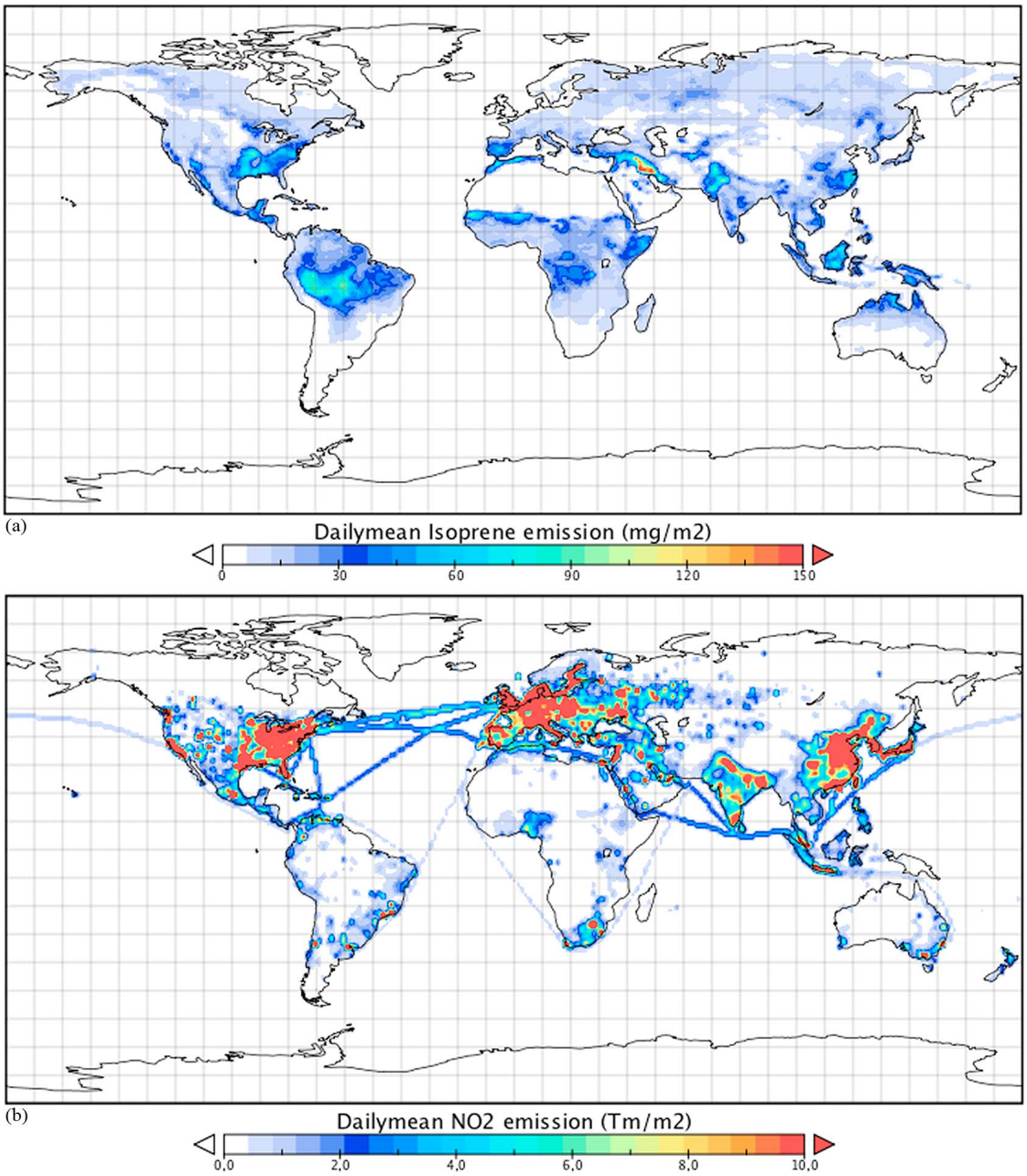

Figure 1. Daily mean emissions of (a) isoprene [mg m^{-2}] and (b) NO_2 [Tg m^{-2}] for July 2004. Isoprene emissions computed with the MEGAN model coupled online within NMMB/BSC-CTM. NO_2 emissions are obtained from the POET database.

[23] Concerning natural on-line emissions, only biogenic emissions are considered as natural source. Biogenic emissions are computed on-line from the Model of Emissions of Gases and Aerosols from Nature (MEGAN) [*Guenther et al.*, 2006]. MEGAN estimates the emission of more than 130 non-methane volatile organic compounds (NMVOCs). All the MEGAN NMVOCs are speciated, following the CB05 chemical mechanism; thus, emissions for isoprene, lumped terpenes, methanol, nitrogen monoxide, acetaldehyde, ethanol, formaldehyde, higher aldehydes, toluene, carbon monoxide, ethane, ethene and paraffin carbon bond, and olefin carbon bond are considered within the chemical processes of the NMMB/BSC-CTM model. Biogenic emissions are computed every hour, accounting for the meteorological evolution changes of solar radiation, surface temperature, moisture and precipitation. Figure 1a shows the daily mean emission of isoprene for July 2004 over the global domain.

3.2. Global Anthropogenic Emissions

[24] Global anthropogenic emissions applied in the present study are based on the *Emmons et al.* [2010] emission database. The majority of the anthropogenic emissions originated from the POET (Precursors of Ozone and their Effects in the Troposphere) database for 2000 (C. Granier et al., POET, a

Table 2. Model Runs

Case Name	Abbreviation	Description
Base case	BC	NMMB/BSC-CTM model with default CB05 chemistry
Crowley and Carl case	CC	NMMB/BSC-CTM model with default CB05 chemistry and the photoexcitation chemistry of NO_2 with the kinetics of *Crowley and Carl* [1997]
Li et al. case	LC	NMMB/BSC-CTM model with default CB05 chemistry and the photoexcitation chemistry of NO_2 with the kinetics of *Li et al.* [2008]

database of surface emissions of ozone precursors, 2005 available at http://www.aero.jussieu.fr/projet/ACCENT/POET.php) [*Olivier et al.*, 2003], which includes anthropogenic emissions (from fossil fuel and biofuel combustion), based on the EDGAR-3 inventory [*Olivier and Berdowsky*, 2001]. For SO_2, anthropogenic emissions are obtained from the EDGAR-FT2000 database. For Asia, these inventories have been replaced by the Regional Emission inventory for Asia (REAS) with the corresponding annual inventory for each emission year [*Ohara et al.*, 2007]. Emissions from 2004 have been selected for the present study. All the anthropogenic emissions are emitted in the first three model layers to account for the sub-grid scale vertical diffusion within the PBL. Hourly emissions are estimated from the monthly mean emission fluxes. Figure 1b shows the daily mean emission of NO_2 for July 2004 over the global domain of study.

3.3. Implementation of the NO_2^* Chemistry

[25] The photoexcitation of NO_2 (reactions (10)–(12)) has been implemented within the CB05 chemical mechanism. The kinetic constant used for reaction (11) is $k_{11} = 2.8 \times 10^{-11}$ cm^3 molecule^{-1} s^{-1} [*Okabe*, 1978; *Crowley and Carl*, 1997]. For reaction (12), two options are implemented: (a) the constant of *Li et al.* [2008] $k_{12} = 1.7 \times 10^{-13}$ cm^3 molecule^{-1} s^{-1}, and (b) the *Crowley and Carl* [1997] kinetic constant upper limit $k_{12} = 1.2 \times 10^{-14}$ cm^3 molecule^{-1} s^{-1}. Thus, three different cases are prepared: a default CB05 without the photoexcitation of NO_2, a CB05 with fast kinetics from *Li et al.* [2008] and a last mechanism with a lower reaction rate constant from *Crowley and Carl* [1997].

[26] In order to consider the photoexcitation of NO_2, the photolysis rate of reaction (10) is computed within the Fast-J photolysis scheme. The quantum yields and cross sections of NO_2 for the production of NO_2^* are obtained from *Atkinson et al.* [2004]. The spectrum is discretized in 7 wavelength bins, where the larger bin includes the photoexcitation part of the spectrum from 412.45 to 850 nm.

[27] The photolysis rate for the photo-dissociation of NO_2 is computed on-line within the NMMB/BSC-CTM model. Results at the first surface model layer for a specific time step show a maximum value for the photolysis rate of $J_{NO2} = 0.6$ min^{-1} and a maximum value for the photoexcitation rate of $J_{NO2*} = 1.6$ min^{-1}.

[28] Additionally, dry-deposition of NO_2^* has also been considered. The approach used is that of *Wesely* [1989] for NO_2. However, tests show that the reaction is fast enough to consider the NO_2^* dry-deposition negligible (not shown).

3.4. Description of the Model Runs

[29] In order to analyze the impact of the NO_2^* chemistry on tropospheric ozone concentration levels at global scale, three model configurations are defined (see Table 2): a Base Case run (BC) with the default CB05 chemical mechanism, a *Crowley and Carl* [1997] Case run (CC) with $k_{12} = 1.2 \times 10^{-14}$ cm^3 molecule^{-1} s^{-1}, and a *Li et al.* [2008] Case run (LC) with $k_{12} = 1.7 \times 10^{-13}$ cm^3 molecule^{-1} s^{-1}. The NMMB/BSC-CTM is configured at a global scale with the dynamics, physics and chemistry described in Table 1.

[30] Thus, three model runs have been performed (BC, CC and LC) for July and August 2004. The horizontal resolution of the global model is $1^\circ \times 1.4^\circ$ and uses 64 vertical sigma-hybrid layers from surface to 0 hPa. The meteorological initial conditions are obtained from the final analysis of NCEP global model for 2004 at 1° horizontal resolution. A spin-up of 6 months was run to prepare the chemical conditions for the July and August 2004 runs. The chemical initial conditions of the spin-up were obtained from the LMDz-INCA2 model [*Szopa et al.*, 2009]. The meteorology is run 24 h and reinitialized each day with the corresponding analysis, while the chemical initial conditions of the next day are those from the previous day model run at 24 h.

3.5. Network of Surface Observations

[31] Background surface observations of O_3, NO_2 and CO are used to evaluate the results of the model NMMB/BSC-CTM. Stations from the World Data Centre for Greenhouse Gases (WDCGG; http://gaw.kishou.go.jp/wdcgg/) have been selected for the evaluation. The WDCGG stations measure O_3, NO_2 and CO in background areas. Moreover, stations from the Co-operative Programme for Monitoring and Evaluation of the Long-range Transmission of Air Pollutants in Europe (EMEP; http://www.emep.int/) have been selected to complement the observations of WDCGG over Europe, and the Clean Air Status and Trends Network (CASTNET; http://java.epa.gov/castnet/) complements the observations over United States of America. Observations of surface O_3 and NO_2 are selected from the EMEP network, while only O_3 observations are obtained from the CASTNET network. The total number of stations used in the evaluation is indicated in Table 5.

[32] Classical statistics are selected to evaluate the model and quantify the impact of the NO_2^* on global air quality. According to the recommendations of the US-EPA a cut-off value of 80 μg m^{-3} is applied to O_3 statistics. The monthly mean model-to-data statistics for the mean bias (MB), root mean square error (RMSE), mean normalized bias error (MNBE), mean normalized gross error (MNGE), mean fractional bias (MFB) and mean fractional error (MFE) are

selected to provide quantitative scores about the performance of the model and the impact of the new photoexcited pathway.

4. Results and Discussion

[33] The impact of the NO_2 photoexcitation chemistry is presented in the following subsections. Specifically, the BC and CC model runs are compared and discussed during July August 2004. These discussions are focused on the northern hemisphere, where major anthropogenic emissions are sourced (see Figure 1b); in addition, this dialog contextualizes recent investigations [*Sarwar et al.*, 2009; *Ensberg et al.*, 2010], that also focused on the northern hemisphere. In addition, LC and CC simulations are also discussed. Furthermore, given the uncertainties inherent to the reaction rate obtained by *Li et al.* [2008] and *Carr et al.* [2009], the impact of the NO_2^* chemistry is assessed by comparing the BC and CC runs.

4.1. Impact of NO_2 Photoexcitation on Surface Ozone

[34] Figure 2 shows the hourly, 8-h average, and daily mean maximum ozone enhancement at surface level when comparing the CC results with the BC results. Results show how the CC chemistry contributes to a maximum increase in the hourly ozone surface concentration around 10–15 ppbv in local urban areas, reaching a maximum of 31 ppbv in Taiwan, and approximately 3–7 ppbv in rural zones. Figure 2b shows the 8-h average maximum enhancements. When compared with the maximum hourly data, it clearly appears a pattern centered on local polluted regions, where the hourly enhancement is about 5 ppbv higher. The new chemistry significantly increases ozone concentrations during its peak hours of formation, which is primarily due to an increase in the production rate of OH radicals. Additionally, the 8-h average concentrations increase 6–8 ppbv in regional continental areas and 8–12 ppbv over water bodies. Major enhancements are observed again in large polluted regions (e.g., southern California area, Florida western coast, northwestern European coast, northern Taiwan, and east China). The daily mean maximum enhancements observed during July and August 2004 (Figure 2c) remain below 7 ppbv over most continental areas of the northern hemisphere. Only in Taiwan, the impact is more relevant and ozone daily mean concentrations may increase more than 15 ppbv.

[35] The areas where the impact of the NO_2 photoexcitation chemistry appears to be relevant are over ocean and sea in agreement with *Sarwar et al.* [2009]. The limited ozone sink processes over water bodies, the shallow marine boundary layer, and the effectiveness of the new rate constant (i.e., by increasing OH production rate) promote higher ozone concentrations. Furthermore, those areas with larger enhancement are characterized by a large NO_x/VOC ratio. Figure 3 shows the maximum value of the ratio NO_x/VOC for July and August at ground level. Indeed, the ship routes are characterized by large NO_x/VOC ratios and strongly contribute to the enhancement of O_3 observed over the oceans. Additionally, enriched NO_y plumes advected from continental areas toward the oceans provides efficient conditions where NO_2^* chemistry plays an important contribution in the background ozone concentrations. Specifically, peroxy acetyl nitrate (PAN) is enhanced when the photoexcitation chemistry is activated. The increase is larger over oceans than over continental areas (not shown), suggesting that the long-range transport of PAN is also an important process that contributes to the enhancement of O_3 over the oceans.

[36] Additionally, atmospheric dynamics over the different ocean areas strongly contributes to the occurrence of ozone enhancements. For instance, the northern Atlantic ocean presents wide areas where ozone enhancements at surface are over 6 ppbv. This behavior is also observed in the northern Pacific ocean, but in this case, the extension where the enhancements reach values over 6 ppbv are not as large as those predicted over the Atlantic. Thus, the impact over continental areas due to the advection of ozone enriched air is more important in Europe (especially northern Europe) than in western USA. While the latter shows important contributions of local emissions, in Europe the background enhanced concentrations overwhelm the local enhancements due to the NO_2^* chemistry. Of significant relevance are the enhancements over the Mexican gulf, the Mediterranean sea, the Persian gulf and the East China sea. Those are areas where atmospheric dynamics play an important role on the accumulation of aged air masses and are affected by large emission sources nearby.

[37] The temporal evolution of the spatially averaged daily mean ozone enhancement over the northern hemisphere, USA, northern Atlantic ocean, Europe, eastern Asia, and the northern Pacific ocean (see Figure 2c) are computed and plotted for the two months analyzed (Figure 4). There is a clear increasing trend in the daily mean enhancements from July to August. In the northern hemisphere, the ozone enhancements go from 2.5 ppbv in the beginning of July to 3 ppbv at the end of August. Such a trend is directly related to the summer climate conditions. The areas where the impact is more marked are the north Atlantic ocean and the north Pacific ocean, where the mean enhancements ranges from 2 to 2.5 ppbv during the two months. There are important increases in ozone enhancements (e.g., during the first week of August in the Pacific ocean) over the oceans. Those are attributed to episodes of strong advection of continental air masses enriched with anthropogenic pollutants. Over continental areas, the enhancement is around 2 ppbv over Europe and USA, and 1.5 ppbv in eastern Asia. Furthermore, Table 3 summarizes the ozone enhancements observed over the different areas. Maximum spatial-averaged enhancements range from 2.6 in the North Atlantic to 1.6 over Asia. It is important to note that also ozone decreases are produced when comparing CC and BC. In this sense, USA, Europe and Asia show ozone decreases of 3.8, 1.5 and 2.3 ppbv respectively. However, the mean behavior in all areas involves an enhancement of O_3.

[38] In order to complement the maximum O_3 enhancements analysis, the number of days where a threshold in the ozone enhancement is exceeded are computed. Table 4 contains the spatially average number of days per region (i.e., North Pacific, USA, North Atlantic, Europe, Asia (see Figure 2c)), and the maximum number of days within a region where an enhancement greater than or equal to 3, 5, 10 or 15 ppbv is modeled. In all areas analyzed, there is always a location that exceeds the 3 ppbv threshold. The North Pacific and USA areas are the ones with more exceedances (up to

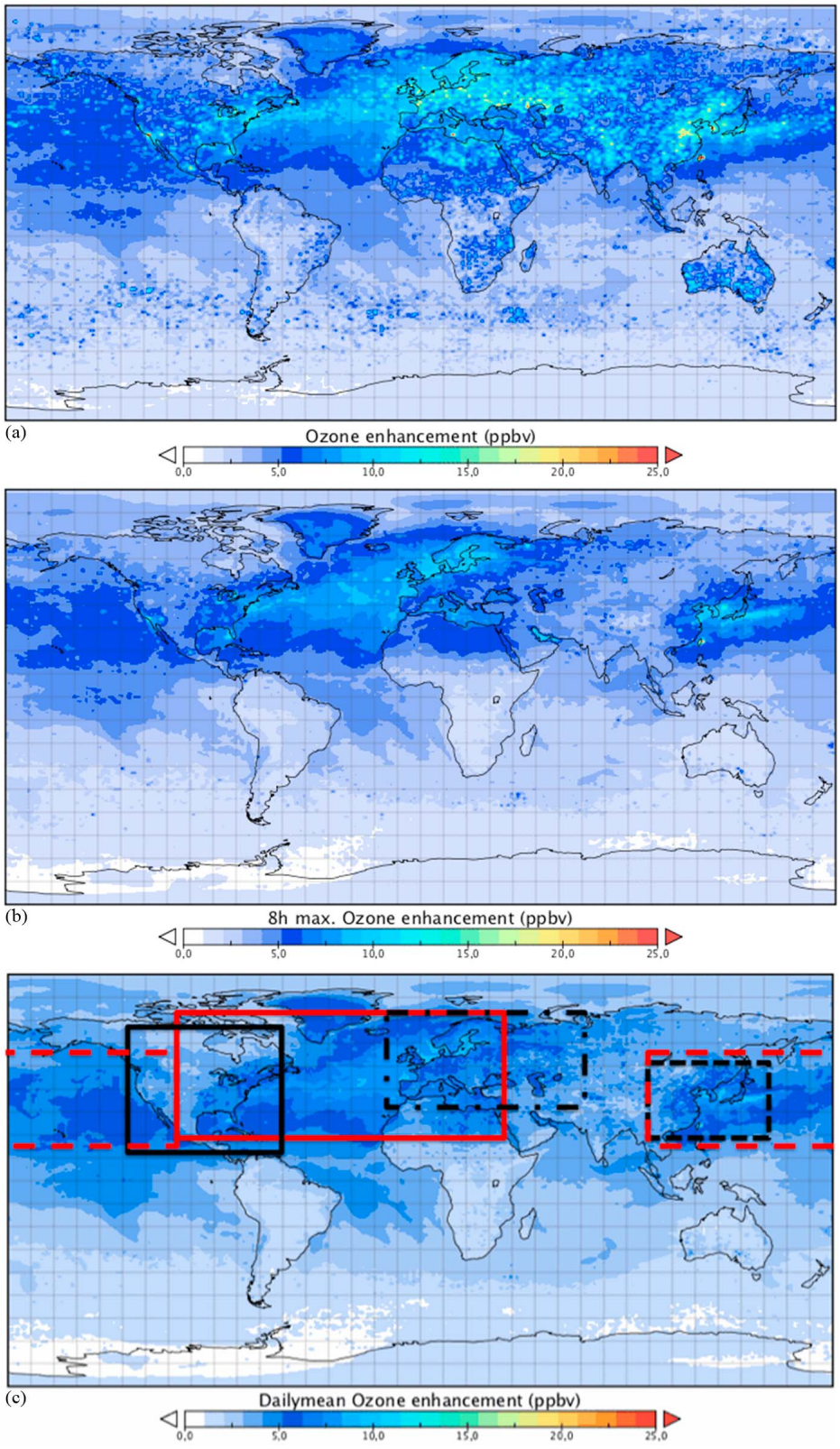

Figure 2. (a) Hourly, (b) 8-h average, and (c) daily mean maximum ozone enhancement at ground level for July and August 2004 due to the inclusion of *Crowley and Carl* [1997] NO_2 photoexcitation chemistry [Lower panel shows the location of the zonal averages for NAtl (red square), EU (dash-dotted black square), Asia (dashed black square), NPacific (dashed red square) and USA (black square) zones].

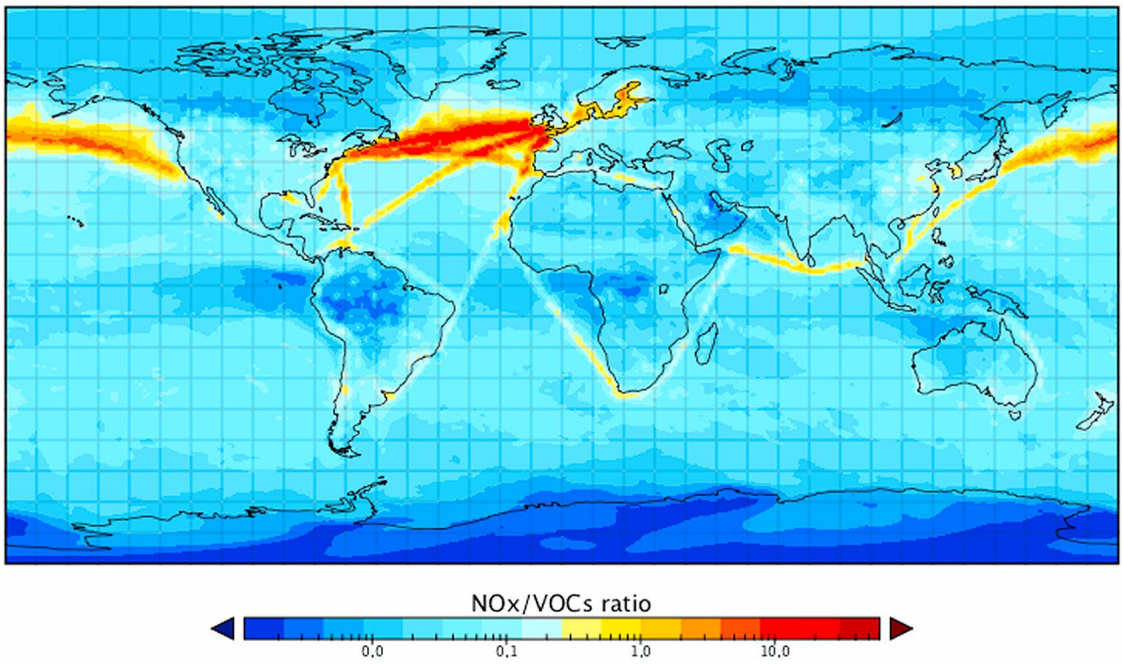

Figure 3. Maximum value of the ratio NOx/VOCs for July August 2004 at ground level.

26 days the threshold of 10 ppbv is exceeded) than the rest of the north hemisphere. The North Atlantic, Europe and Asia zones present the lowest number of days with high exceedances (10 and 15 ppbv).

[39] Compared with other studies focused on the NO_2^* chemistry reported over USA, *Sarwar et al.* [2009] showed a maximum increase in O_3 concentrations of 9 ppbv in eastern USA and 6 ppbv in western USA for July 2001 and 2002, and *Ensberg et al.* [2010] reported maximum increases in the 8-h average O_3 concentrations of 8 ppbv for the South Coast Air Basin of California for summer conditions of 2005. Results are in agreement with those previous simulations. However, the impact of the new chemistry is more relevant downwind of important polluted areas, and there is an important effect on the long-range transport chemistry over the oceans. Note, the marked enhancements within the air masses advected from the eastern USA coast toward Europe, and from the eastern Asian coast toward western USA within 20°N and 70°N latitude. *Sarwar et al.* [2009] already noted a major impact over water bodies. Results exemplify the fact that ozone enhancements are more pronounced over the oceans. Additionally, results over east Asia

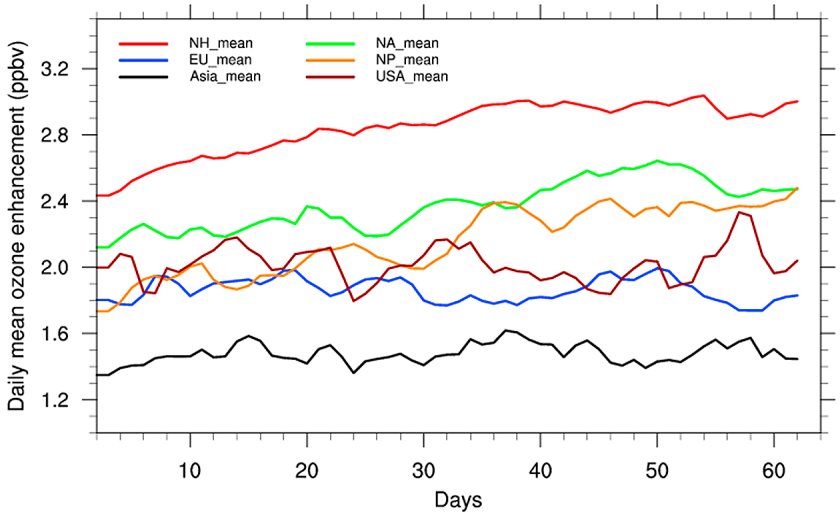

Figure 4. Temporal evolution of the daily mean ozone enhancement spatially averaged over Northern hemisphere (NH_mean), Europe (EU_mean), Asia (Asia_mean), North Atlantic Ocean (NA_mean), North Pacific Ocean (NP_mean), and USA (USA_mean) at ground level for July August 2004 due to the inclusion of *Crowley and Carl* [1997] NO_2 photoexcitation chemistry [The location of the averaged areas are plotted in Figure 2].

Table 3. Daily Mean Ozone Enhancement Over Several Areas Around the World Depicted in Figure 2

Area	Surface Ozone Enhancement (ppbv)		
	Minimum	Average	Maximum
North Pacific	0.8	2.1	2.5
USA	−3.8	1.9	2.3
North Atlantic	0.5	2.3	2.6
Europe	−1.5	1.8	2.0
Asia	−2.3	1.4	1.6

are in concordance with *Li et al.* [2011] who reported enhancements over 30 ppbv in major urban areas. Differences between the present results and those from *Sarwar et al.* [2009], *Ensberg et al.* [2010], and *Li et al.* [2011] are mainly attributed to different model resolution (e.g., mesoscale applications compared against global runs), and emission inventories.

[40] Focusing in strong NO_x emission sources, the temporal evolution of the surface ozone concentration in Los Angeles, New York, Paris and Beijing are plotted in Figure 5 for July and August 2004. The hourly concentrations for both the BC and CC are plotted. As noted before, the main differences are observed during peak ozone formation hours. The CC case shows larger ozone concentrations during midday for the two months in all the mega-cities selected. A marked enhancement at noon and a rather slow loss rate of ozone during nighttime are the main impacts of the photoexcited chemistry in strongly polluted areas. Not all days during the two-month time frame show similar enhancements, which is primarily due to meteorological conditions that may lead to strong or weak enhancements during a particular day; i.e., meteorological conditions may sometime dominate gas-phase chemistry, which in turn, can either increase or decrease concentrations of atmospheric species at a given pressure level.

4.1.1. Influence on NO_2, HONO and OH Surface Concentrations Compared to O_3

[41] The photoexcitation of NO_2 promotes the production of HONO and OH radical through pathway described by reaction (12). This new source of HONO during daytime may contribute to the enhancement of the OH radical and thus the oxidative capacity of the atmosphere, while, also furthering the production of ozone. On the other hand, the NO_2^* chemistry may contribute to the loss of available NO_x in the atmosphere. The BC and CC model runs are used to compare the enhancements and loss of O_3, NO_2, HONO, and OH. Figure 6 shows the maximum decreases and enhancement of daily mean O_3, NO_2, HONO and OH for the period studied.

[42] As stated previously, the CC case exhibits ozone enhancements over the entire globe. However, one can also identify regions where O_3 concentrations slightly decrease (Figure 6a). Especially relevant is the result over Australia, where minor O_3 enhancements are observed (below 3 ppbv) in addition to non-negligible decreases in O_3 concentrations (1–2 ppbv). It is important to note that these decreases are observed during the cold season in the Australian continent. The northern hemisphere also exhibits regions where O_3 decreases with the inclusion of *Crowley and Carl* [1997] kinetics, being the most relevant in northeast India (1–2.5 ppbv). This region is characterized by low NO_x and biogenic emissions, suggesting remote transport of low NO_x air masses.

[43] Figure 6d shows the maximum enhancement of NO_2 when comparing the CC and BC runs. Overall increases in NO_2 are expected due to the increased oxidation rate associated to reaction (12). Over background regions, the impact of the NO_2^* chemistry is negligible less than 0.01 ppbv. During the daytime, the photoexcitation chemistry contributes to an overall enhancement of the surface NO_2. In areas affected by significant NO_x emissions, the enhancements during the day reach maximum values of 1–6 ppbv. On the other hand, during nighttime, those areas are characterized by a decrease in NO_2 concentrations in the CC case. Unlike O_3, NO_2 variations due to the new kinetics are strongly associated to large NO_x emission sources. In this sense, Figures 6c and 6d show a strong correlation with Figure 1b where NO_2 emissions are depicted. The maximum decrease in NO_2 is observed in east Asia, where loss of 4 ppbv in NO_2 is obtained with the simulations.

[44] The CC case shows an increasing trend in HONO concentrations during most part of the day although the variations are considerably small (Figure 6f). Maximum enhancements and decreases are observed in/near urban locations of 8–9 and 6–7 pptv, respectively. In background regions, the CC simulation shows small HONO enhancements during most of the day, meanwhile the areas influenced by large NO_x emissions present an enhancement during the day and a loss of HONO during the nighttime. The major loss rate is observed during the first daylight hours followed by a sudden enhancement of HONO (not shown). These results indicate that the impact of the NO_2^* chemistry on NO_2 and HONO is negligible.

[45] One of the major results of the photoexcited chemistry is the production of the hydroxyl radical following the direct formation through reaction (12) and through the photolysis of HONO via reaction (4). Figure 6h presents the maximum enhancement of OH for the two months studied. The spatial patterns are rather similar to those associated with O_3 impacts (Figure 6b). The areas where the enhancement is more relevant are those located over water bodies and affected by direct NO_x emissions (e.g., ship routes, large industrial areas, urban areas). The maximum enhancement observed in the CC case is around $\sim 6–7 \times 10^{-2}$ pptv ($14–17 \times 10^5$ molec cm^{-3}), which are produced during daylight hours. In background continental areas, results show limited

Table 4. Number of Days With Exceedances of the Enhancement Threshold Values for Hourly Ozone Concentration at Ground Level Over Several Areas Around the World Depicted in Figure 2c[a]

Area	Average/Maximum (days)			
	≥3 ppbv	≥5 ppbv	≥10 ppbv	≥15 ppbv
North Pacific	14.5/62	1.7/62	0.06/26	0.01/3
USA	39.2/62	9/62	0.12/26	0.01/3
North Atlantic	21.6/62	6.7/56	0.1/6	0.01/3
Europe	32.5/62	7.9/52	0.24/6	0.05/3
Asia	23.6/62	2.9/48	0.19/5	0.03/2

[a]Average: number of days exceeding a threshold spatially averaged over an area (over all grids of an area); Maximum: the maximum number of days exceeding a threshold in a specific grid of an area of study.

Table 5. Model Evaluation for July and August 2004 for the Base Case Run (BC) and Crowley and Carl Run (CC)

Network	Number of Stations	Observed Mean (ppbv)	Model Mean (ppbv)	MB (ppbv)	RMSE (ppbv)	MNBE (%)	MNGE (%)
			Surface O_3 Statistics (BC/CC)				
WDCGG	41	31.7	27.3/30.9	−4.3/−0.8	11.2/10.9	−7.8/4.2	25.5/27.3
EMEP	70	38.3	27.3/31.1	−11/−7.2	15.8/14.0	−24.2/−13.4	30.4/28.0
CASTNET	63	31.7	33.8/37.5	2.4/5.8	2.2/10.4	11.6/23.8	22.7/30.1
			Surface NO_2 Statistics (BC/CC)				
WDCGG	12	1.9	1.2/1.2	−0.7/−0.7	2.0/2.0	29.4/33.2	102.3/102.3
EMEP	21	3.9	1.8/1.8	−2.1/−2.1	3.4/3.4	−38.9/−37.9	56.6/55.8
			Surface CO Statistics (BC/CC)				
WDCGG	14	121.5	145.3/139.8	23.8/18.3	51.5/49.1	43.3/37.8	50.1/47.1

enhancements during the daytime. Furthermore, it is important to note that in some areas a decrease in the OH radical is also observed (detected during the last daylight hours) (Figure 6g). The ship routes from east USA toward Europe are the regions where the decrease of OH is more remarkable when the photoexcitation chemistry is turned on. The OH radical is extremely reactive, and its concentration in atmospheric conditions range from 8×10^{-3} to 0.5 pptv. Thus, the variations observed in the atmospheric equilibrium concentrations are understandably small due to its high reactivity.

4.2. Vertical Distribution of the Ozone Enhancements Due to the NO_2^* Chemistry

[46] Vertical mixing and convective transport are efficient processes to transport surface emission and polluted air masses toward upper layers. The ozone enhancement observed at the ground level is also observed throughout the troposphere. Figure 7 presents the vertical cross sections of the maximum hourly O_3 enhancement for July and August 2004 at 90W, 30W, 10E and 130E longitude degrees. As noted in the previous sections, the main impacts are produced in the northern hemisphere, from 10N to 70N latitude degrees. Figures 7a and 7c depicts a well mixed vertical layer within the boundary layer, which contributes to the vertical transport of the O_3 enhancement from the surface up to 700 hPa (∼3000 m a.s.l.). This vertical mixing is more efficient over continental areas than over water bodies since the vertical distribution over water bodies is due to the advection of well-mixed continental air masses within the PBL and, in some cases, transported beyond it via convective updrafts. The vertical distribution shows an ozone enhancement around 10–20 ppbv in the lower troposphere. Some of the enhancement observed in upper layers is attributed to local surface emissions (i.e., latitudes 50N-60N in Figure 7c, where northern Europe emissions strongly influence the enhanced O_3 profile). However, the synoptic transport of enriched air masses from strong emission sources toward the

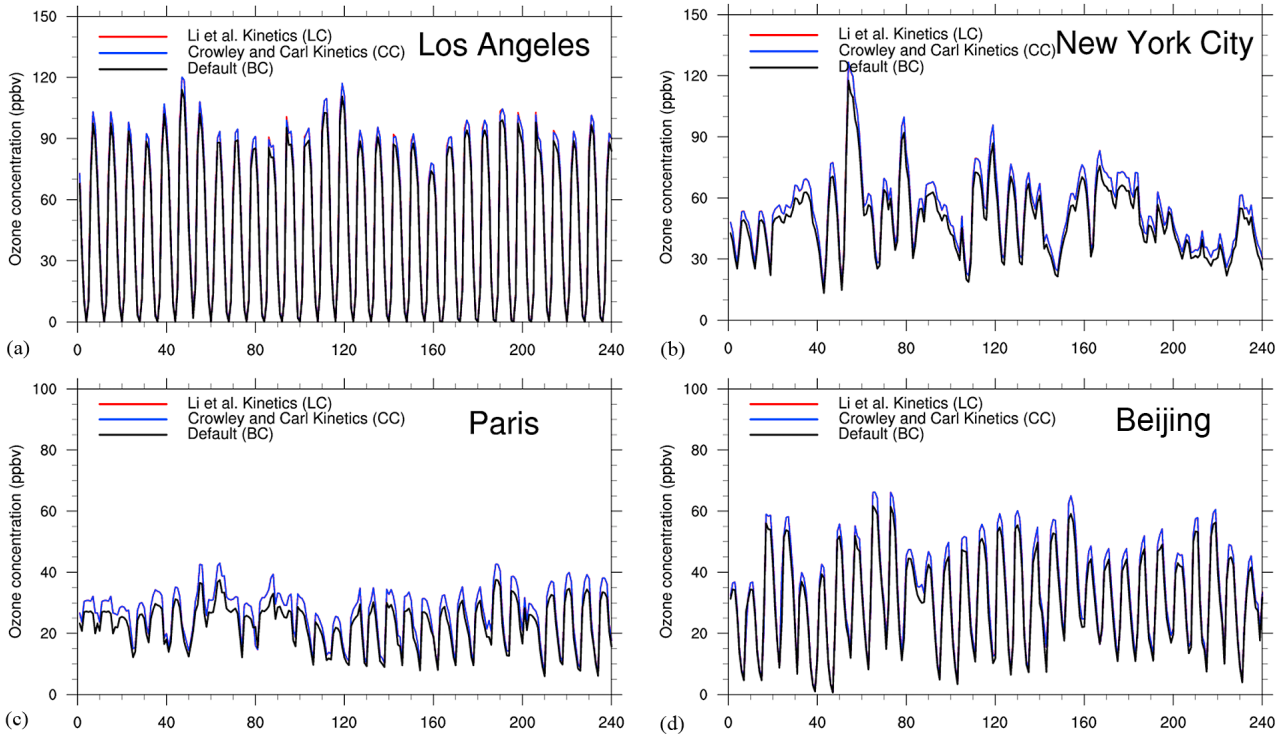

Figure 5. Temporal evolution of the hourly ozone concentration in several mega-cities for July 2004 from BC, CC and LC cases. (a) Los Angeles, (b) New York, (c) Paris, and (d) Beijing.

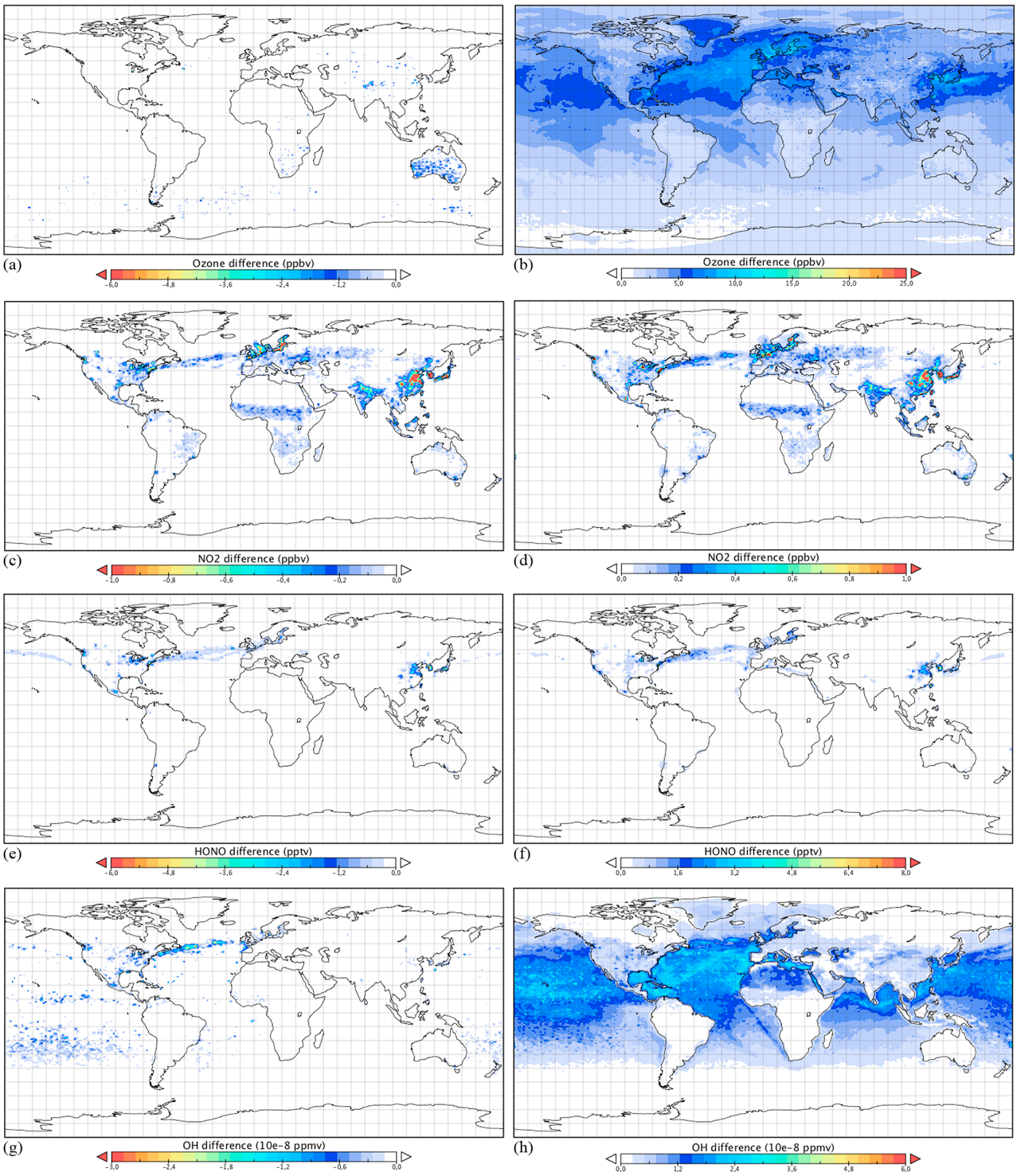

Figure 6. Maximum daily mean (a, c, e, g) decreases and (b, d, f, h) enhancements in near-ground level concentrations for O_3 (Figures 6a and 6b), NO_2 (Figures 6c and 6d), HONO (Figures 6e and 6f) and OH (Figures 6g and 6h) for July and August 2004 due to the inclusion of *Crowley and Carl* [1997] NO_2 photoexcitation chemistry.

ocean in the lower and middle troposphere is also a relevant process when assessing the impact of the new chemistry. The cross sections over the Atlantic ocean and the western Pacific clearly depicts a uniform air mass, where the maximum enhancements are 8–9 ppbv. These air masses extend from the surface to about 650 hPa or, in some cases, cover the entire troposphere when approaching the North Pole.

[47] The vertical distribution of atmospheric species contributes to the intercontinental transport of polluted air masses. The horizontal extension of the enriched air masses involved

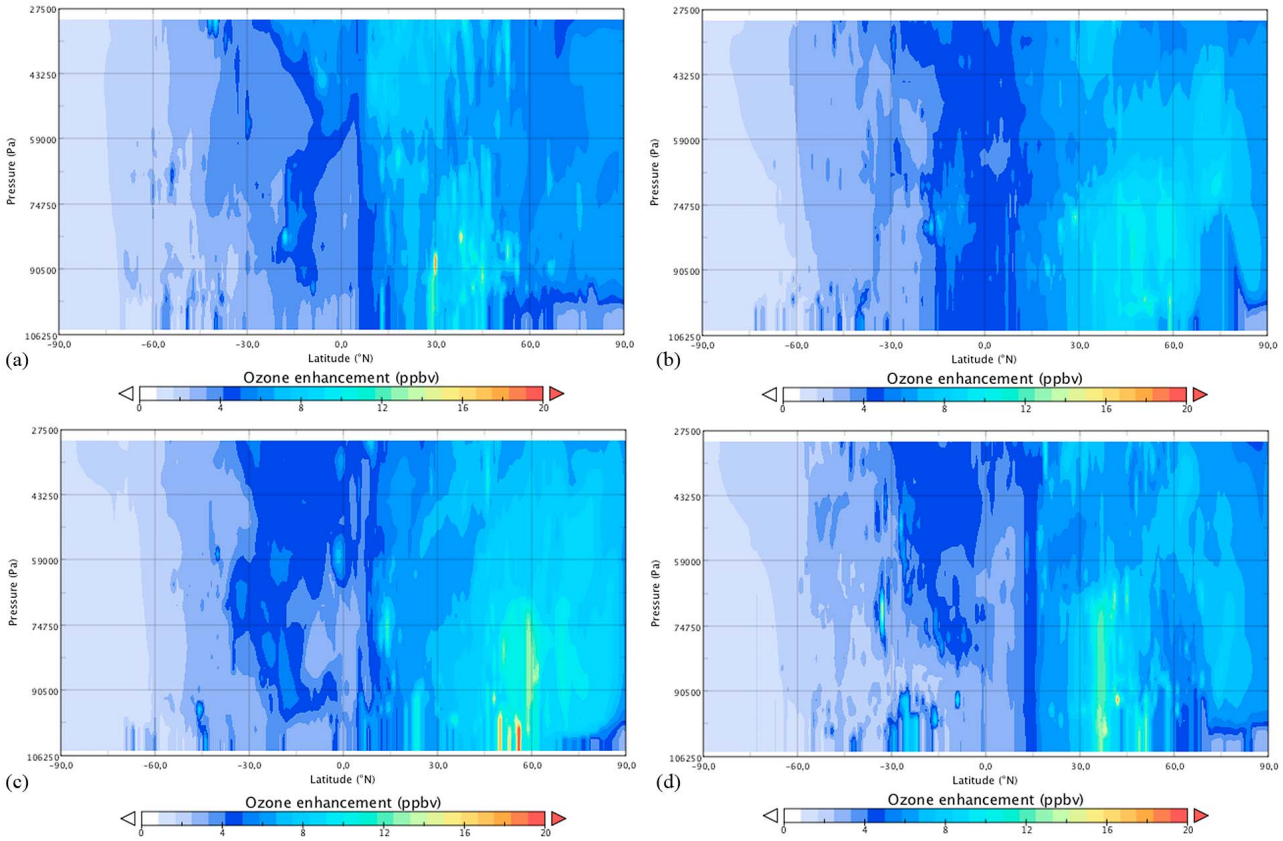

Figure 7. Vertical cross sections of the maximum hourly enhancement concentrations for O_3 at longitude (a) 90W, (b) 30W, (c) 10E, and (d) 130E.

in this intercontinental transport from USA to Europe, and Asia to USA is rather constant within the troposphere. Over the Atlantic (see Figure 7b), a core region, located between 35N and 65N from the surface to 650 hPa shows an enrichment of 8–10 ppbv of ozone. Such air masses strongly contribute to the O_3 concentrations modeled over Europe.

4.3. Differences in the Impact of Li et al. and Crowley and Carl Kinetic Reaction for the Photoexcitation of NO_2 in Presence of Water Vapor

[48] Given the unresolved differences between past studies that have measured the reaction rate of NO_2^* with H_2O and the comparable results of *Crowley and Carl* [1997] and *Carr et al.* [2009], the CC and LC model runs are compared for the sake of completeness. Future studies are needed to determine conclusively that NO_2 photoexcitation chemistry indeed occurs under atmospheric conditions. LC and CC cases have been run for July and August 2004. Figure 8a presents the maximum 8-h average ozone difference between cases LC and CC. The first striking result is their similar behavior in background areas. Contrary to initial expectations, the different kinetic rate for reaction (12) of LC and CC, under near-ground level atmospheric conditions, produce similar results in most locations. Major differences, however, appear where large emissions are present. In such places, results show enhancements of 3–6 ppbv in western Europe, western and eastern USA coasts, and Asia. Moreover, in areas with large anthropogenic emissions, like California, northeastern USA, the Baltic sea, the Korean peninsula or China show larger enhancements around 10 ppbv when using the *Li et al.* [2008] kinetics. Such enhancements are strongly localized in highly polluted areas. Furthermore, Figure 8b shows the 8h-average mean ozone difference between LC and CC for the two months studied. Results show a limited impact when comparing the LC and CC simulations; as stated above, only highly polluted areas show significant mean differences, which remain below 3 ppbv.

[49] Focusing on ozone concentrations in mega-cities, Figure 5 plots the surface ozone temporal evolution of the LC, CC and BC cases. In most situations, LC results behave similar to those produced by the CC case, with an enhancement of several ppbv, compared with the BC. There is no clear difference between results from LC and CC. Namely, the limiting pathway in the photoexcitation of NO_2 is through reaction (10), and the effect of reaction (12) is limited within this context. Under a large variation of atmospheric conditions and emission scenarios, both chemistries, LC and CC, behaves similarly. Only in a few regions, LC produces significant enhancements (below 3 ppbv) when compared to CC. For instance, the South Coast air basin of California presents some enhancements downwind Los Angeles city, while in Los Angeles no relevant differences exist (in agreement with [*Ensberg et al.*, 2010] results in Los Angeles, Pomona and Riverside).

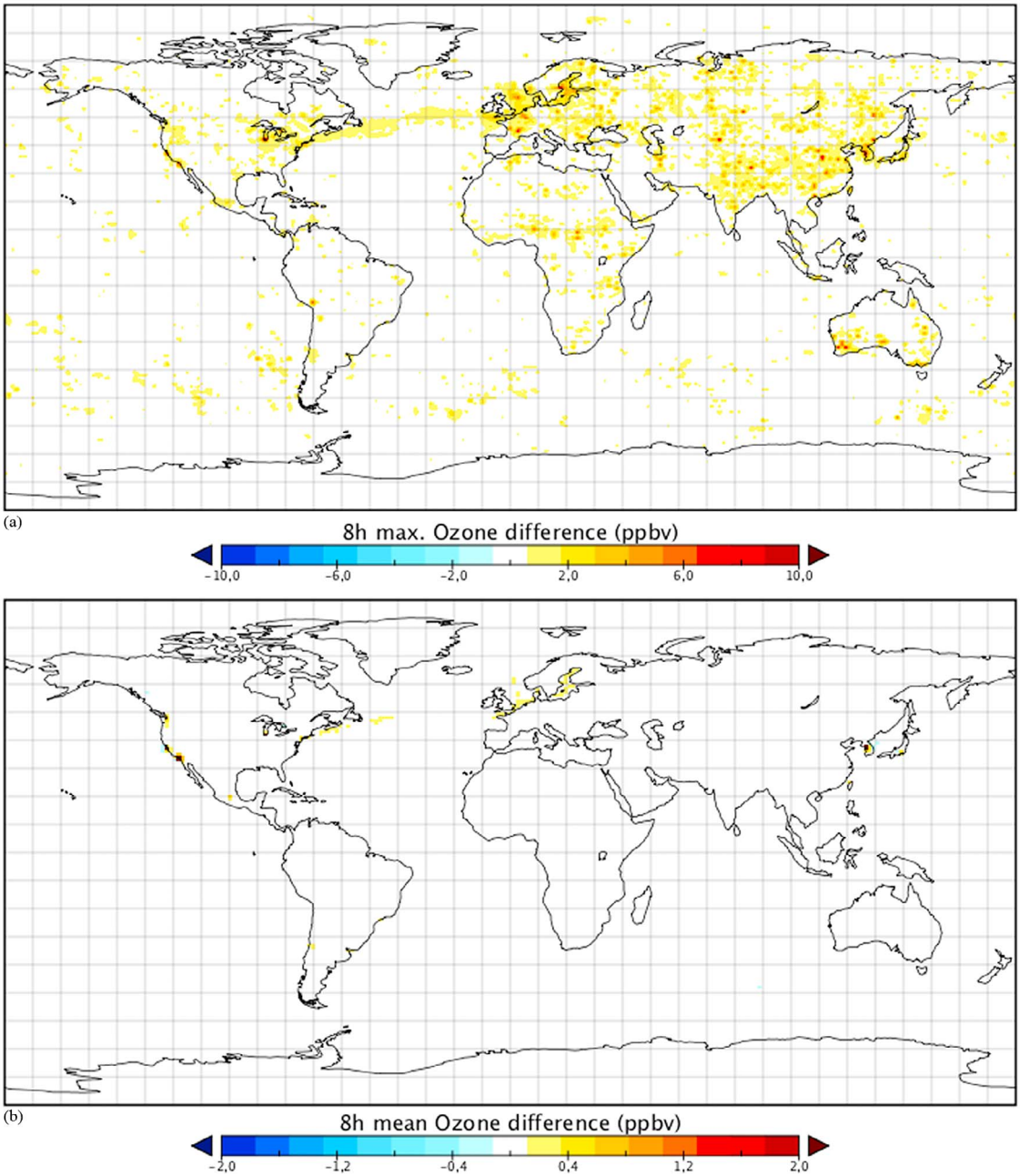

Figure 8. (a) 8h-average maximum and (b) 8h-average mean ozone difference between [*Li et al.*, 2008] and [*Crowley and Carl*, 1997] chemistries for July and August 2004.

4.4. Evaluation Metrics With and Without the Photoexcited NO_2 Chemistry

[50] All the enhancements discussed in the previous section impact the model performance. Table 5 presents some classical statistics for ground level O_3, NO_2 and CO from BC and CC model cases. Three different background networks are used. The number of stations per network are provided in the second column of the table. The O_3 model mean for July and August 2004 at surface level increases from 27.3 ppbv to 30.9 ppbv with the CC case when using the WDCGG observation network. Similar trends are obtained when the EMEP and the CASTNET network are used. The largest increase is observed with the CASTNET stations, the model mean increases from 33.9 to 37.5 ppbv. Those model mean increases have a positive impact in the EMEP and WDCGG networks statistics but an increase of the bias and the error is then produced in the CASTNET network.

[51] When NO_2 and CO are evaluated, the effect of the new chemistry produces a rather positive impact on the statistical metrics. Both, bias and error are slightly reduced. The reduction is more significant for CO than NO_2.

5. Summary and Conclusions

[52] For the first time, the impact of NO_2^* chemistry is assessed at a global scale, during the July August 2004, by

using the new online NMMB/BSC-CTM air quality model. *Li et al.* [2008] suggested that the reaction of the photoexcited NO_2 with H_2O may be a significant contributing source of OH radicals under atmospheric conditions. They reported a reaction rate for NO_2^* with H_2O, which is an order of magnitude greater than what it was previously reported in the literature by *Crowley and Carl* [1997]. Following the idea of a new OH source from NO_2^* with H_2O, several authors have studied the impact on air quality over the USA [e.g., *Wennberg and Dabdub*, 2008; *Sarwar et al.*, 2009; *Ensberg et al.*, 2010]. Here, a sensitivity study of the photoexcited NO_2 is discussed by means of three main cases: a default case without the photoexcitation chemistry, a second case with the photoexcitation of NO_2 implemented following *Crowley and Carl* [1997] kinetic rates, and a third case using the rate suggested by *Li et al.* [2008].

[53] Results show a general enhancement of O_3 when the photoexcited chemistry is applied. At ground level over continental areas, a maximum enhancement of 5–15 ppbv is modeled, and over water bodies the daily mean O_3 concentration increase between 8–12 ppbv. Europe, Asia and eastern USA present the largest impacts on ground level O_3. Under highly polluted conditions, the enhancement can reach a maximum of 31 ppbv, e.g. Taiwan. Even though, the photoexcited chemistry has a strong influence on O_3 and its precursors at the surface, the vertical mixing of enriched NO_x air masses contributes to increase the OH production within the PBL. Thus, O_3 is enhanced by 10–15 ppbv within the first 3000 m of atmosphere. Vertical transport appears to be an efficient process to vertically distribute the impact of the photoexcited NO_2 chemistry.

[54] The impact on NO_2, HONO and OH has been also analyzed. While the enhancement of NO_2 and HONO is delimited over strongly polluted emission areas, OH radicals presents a clear distributed pattern over the oceans. Also, in regions where the NOx/VOCs ratio is large, the enhanced of OH and O_3 is favored. Another relevant result of the sensitivity analysis is the modest impact of the photoexcitation of NO_2 on HONO concentrations. Overall, small increases of HONO are observed with a maximum enhancement of 8–9 pptv in urban locations.

[55] *Crowley and Carl* [1997] and *Li et al.* [2008] NO_2^* kinetics are compared. Results indicate O_3 enhancements of the 8h-average mean in the LC case of 2 ppbv over areas with high NOx/VOCs ratio while the impact in the rest of the domain is lower. Maximum differences are observed over hot spot locations, where high NO_x emissions are present. Around those areas, maximum enhancements of 5–10 ppbv are identified in the LC case. In conclusion, selecting a fast kinetic rate or a slower one does not result in large differences of O_3 enhancements in most areas, only in regions of high NO_x emissions.

[56] Results obtained here complement analysis of the impact of including the NO_2 photoexcitation chemistry on air quality [*Wennberg and Dabdub*, 2008; *Sarwar et al.*, 2009; *Ensberg et al.*, 2010; *Li et al.*, 2011]. From a global perspective, not only local areas are impacted by that new chemistry, but background regions and intercontinental transport are strongly affected. In this sense, further analysis is required to elucidate the impact of this chemistry on air quality at higher resolution over regions like Europe and Asia, where the response of secondary pollutants seems to be significant. Furthermore, the global results are in agreement with the previous reported [e.g., *Wennberg and Dabdub*, 2008; *Sarwar et al.*, 2009; *Ensberg et al.*, 2010; *Li et al.*, 2011] over USA and China, allowing for a multiscale analysis in other areas also.

[57] **Acknowledgments.** The authors wish to thank WOUDC, GAW, EMEP, CASTNET-EPA for the provision of measurement stations. Also, thanks to S. Szopa and A. Cozic for the provision of LMDz-INCA2 chemical data as initial chemical conditions. This work is funded by grants CGL2008-02818-CLI and CGL2010-19652 of the Spanish Ministry of Economy and Competitiveness. All the numerical simulations were performed with the MareNostrum Supercomputer hosted by the Barcelona Supercomputing Center.

References

Amedro, D., A. Parker, C. Schoemaecker, and C. Fittschen (2011), Direct observation of OH radicals after 565 nm multi-photon excitation of NO_2 in the presence of H_2O, *Chem. Phys. Lett.*, *513*(1–3), 12–16.

Atkinson, R., D. Baulch, R. Cox, J. Crowley, R. Hampson, R. Hynes, M. Jenkin, M. Rossi, and J. Troe (2004), Evaluated kinetic and photochemical data for atmospheric chemistry: I. Gas phase reactions of O_x, HO_x, NO_x and SO_x species, *Atmos. Chem. Phys*, *4*, 1461–1738.

Betts, A. (1986), A new convective adjustment scheme. Part I: Observational and theoretical basis, *Q. J. R. Meteorol. Soc.*, *112*(473), 677–691.

Betts, A., and M. Miller (1986), A new convective adjustment scheme. Part II: Single column tests using GATE wave, BOMEX, ATEX and Arctic air-mass data sets, *Q. J. R. Meteorol. Soc.*, *112*(473), 693–709.

Byun, D., and J. Ching (1999), *Science Algorithms of the EPA Models-3 Community Multiscale Air Quality (CMAQ) Modeling System*, Off. of Res. and Dev., U.S. Environ. Prot. Agency, Washington, D. C.

Carr, S., D. Heard, and M. Blitz (2009), Comment on "Atmospheric hydroxyl radical production from electronically excited NO_2 and H_2O," *Science*, *324*(5925), 336.

Crowley, J., and S. Carl (1997), OH formation in the photoexcitation of NO_2 beyond the dissociation threshold in the presence of water vapor, *J. Phys. Chem. A*, *101*(23), 4178–4184.

Ek, M. B., K. E. Mitchell, Y. Lin, E. Rogers, P. Grunmann, V. Koren, G. Gayno, and J. D. Tarpley (2003), Implementation of Noah land surface model advances in the National Centers for Environmental Prediction operational mesoscale Eta model, *J. Geophys. Res.*, *108*(D22), 8851, doi:10.1029/2002JD003296.

Emmons, L., et al. (2010), Description and evaluation of the Model for Ozone and Related Chemical Tracers, version 4 (MOZART-4), *Geosci. Model Dev.*, *3*, 43–67.

Ensberg, J., M. Carreras-Sospedra, and D. Dabdub (2010), Impacts of electronically photo-excited NO_2 on air pollution in the South Coast Air Basin of California, *Atmos. Chem. Phys.*, *10*, 1171–1181.

Fels, S., and M. Schwarzkopf (1975), The simplified exchange approximation—A new method for radiative transfer calculations, *J. Atmos. Sci.*, *32*, 1475–1488.

Ferrier, B. S., Y. Jin, Y. Lin, T. Black, E. Rogers, and G. DiMego (2002), Implementation of a new grid-scale cloud and precipitation scheme in the NCEP Eta model, paper presented at 15th Conference on Numerical Weather Prediction, Am. Meteorol. Soc., San Antonio, Tex.

Foley, K., S., et al. (2010), Incremental testing of the Community Multiscale Air Quality (CMAQ) modeling system version 4.7, *Geosci. Model Dev.*, *3*, 205–226.

Gery, M., G. Whitten, J. Killus, and M. Dodge (1989), A photochemical kinetics mechanism for urban and regional scale computer modeling, *J. Geophys. Res.*, *94*(12), 12,925–12,956.

Guenther, A., T. Karl, P. Harley, C. Wiedinmyer, P. Palmer, and C. Geron (2006), Estimates of global terrestrial isoprene emissions using MEGAN (Model of Emissions of Gases and Aerosols From Nature), *Atmos. Chem. Phys. Discuss.*, *6*, 107–173.

Janjic, Z. (1977), Pressure gradient force and advection scheme used for forecasting with steep and small scale topography, *Beitr. Phys. Atmos.*, *50*(1), 186–199.

Janjic, Z. (1979), Forward-backward scheme modified to prevent two-grid-interval noise and its application in sigma coordinate models, *Contrib. Atmos. Phys*, *52*, 69–84.

Janjic, Z. (1984), Nonlinear advection schemes and energy cascade on semi-staggered grids, *Mon. Weather Rev.*, *112*(6), 1234–1245.

Janjic, Z. (1990), The step-mountain coordinate: Physical package, *Mon. Weather Rev.*, *118*, 1429–1443.

Janjic, Z. (1994), The step-mountain Eta coordinate model: Further developments of the convection, viscous sublayer, and turbulence closure schemes, *Mon. Weather Rev.*, *122*(5), 927–945.

Janjic, Z. (2000), Comments on "Development and evaluation of a convection scheme for use in climate models," *J. Atmos. Sci.*, *57*(21), 3686–3686.

Janjic, Z. (2001), Nonsingular implementation of the Mellor-Yamada level 2.5 scheme in the NCEP meso model, *Off. Note 437*, Natl. Cent. for Environ. Predict., Natl. Weather Serv., NOAA, Camp Springs, Md.

Janjic, Z. (2003), A nonhydrostatic model based on a new approach, *Meteorol. Atmos. Phys.*, *82*(1), 271–285.

Janjic, Z. (2005), A unified model approach from meso to global scales, *Geophys. Res. Abstr.*, *7*, 24–29.

Janjic, Z., and T. Black (2007), An ESMF unified model for a broad range of spatial and temporal scales, in *Geophys. Res. Abstr.*, *9*, Abstract 05025.

Janjic, Z., H. Huang, and S. Lu (2009), A unified atmospheric model suitable for studying transport of mineral aerosols from meso to global scales, in *Earth and Environmental Science*, *IOP Conf. Ser.*, *7*, 6.

Janjic, Z., T. Janjic, and R. Vasic (2011), A class of conservative fourth-order advection schemes and impact of enhanced formal accuracy on extended-range forecasts, *Mon. Weather Rev.*, *13*(5), 1556–1568.

Jorba, O., C. Pérez, K. Karsten, Z. Janjic, D. Dabdub, and J. Baldasano (2009), Development of an integrated chemical weather prediction system for environmental applications at meso to global scales: NMMB/BSC-CHEM, paper presented at 9th Annual Meeting, Eur. Meteorol. Soc., Toulouse, France, 28 Sept. to 2 Oct.

Jorba, O., C. Pérez, K. Haustein, Z. Janjic, J. Baldasano, D. Dabdub, A. Badia, and M. Spada (2011), The NMMB/BSC-CTM: A multiscale online chemical weather prediction system, in *HARMO 14: Proceedings of the 14th International Conference on Harmonisation Within Atmospheric Dispersion Modelling for Regulatory Purposes*, vol. 14, pp. 345–349, Dep. of Mech. Eng., Univ. of Environ. Technol. Lab., Univ. of West Macedonia, Thessaloniki, Greece.

Lacis, A., and J. Hansen (1974), A parameterization for the absorption of solar radiation in the Earth's atmosphere, *J. Atmos. Sci.*, *31*, 118–133.

Leighton, P. (1961), *Photochemistry of Air Pollution*, vol. 9, Academic, New York.

Li, S., J. Matthews, and A. Sinha (2008), Atmospheric hydroxyl radical production from electronically excited NO_2 and H_2O, *Science*, *319*(5870), 1657–1660.

Li, S., J. Matthews, and A. Sinha (2009), Response to comment on "Atmospheric hydroxyl radical production from electronically excited NO_2 and H_2O," *Science*, *324*(5925), 336.

Li, Y., J. An, M. Min, W. Zhang, F. Wang, and P. Xie (2011), Impacts of HONO sources on the air quality in Beijing, Tianjin and Hebei province of China, *Atmos. Environ.*, *45*, 4735–4744.

Monin, A., and A. Obukhov (1954), Osnovnye zakonomernosti turbulentnogo peremesivanija v prizemnom sloe atmosfery, *Tr. Geofiz. Inst. Akad. Nauk SSSR*, *24*, 163–187.

Ohara, T., H. Akimoto, J. Kurokawa, N. Horii, and K. Yamaji (2007), An Asian emission inventory of anthropogenic emission sources for the period 1980–2020, *Atmos. Chem. Phys*, *7*, 4419–4444.

Okabe, H. (1978), *Photochemistry of Small Molecules*, John Wiley, New York.

Olivier, J., and J. Berdowsky (2001), Global emission sources and sinks, in *The Climate System*, pp. 33–77, A. A. Balkema, Lisse, Netherlands.

Olivier, J., J. Peters, C. Granier, G. Petron, J. Müller, and S. Wallens (2003), Present and future surface emissions of atmospheric compounds, *POET Rep. 2*, Atmos. Compos. Change, Univ. di Urbino, Urbino, Italy.

Pérez, C., J. Baldasano, P. Jiménez-Guerrero, O. Jorba, K. Haustein, E. Cuevas, S. Basart, and S. Nickovic (2009), Dust modelling and forecasting in the Barcelona Supercomputing Center: Activities and developments, in *Earth and Environmental Science*, *IOP Conf. Ser.*, *7*, 012013, doi:10.1088/1755-1307/7/1/012013.

Pérez, C., et al. (2011), Atmospheric dust modeling from meso to global scales with the online NMMB/BSC-Dust model—Part 1: Model description, annual simulations and evaluation, *Atmos. Chem. Phys.*, *11*, 13,001–13,027.

Sander, S., et al. (2006), Chemical kinetics and photochemical data for use in atmospheric studies evaluation number 15, *JPL Publ. 06-2*, 153 pp.

Sarwar, G., R. Pinder, K. Appel, R. Mathur, and A. Carlton (2009), Examination of the impact of photoexcited NO_2 chemistry on regional air quality, *Atmos. Environ.*, *43*(40), 6383–6387.

Simmons, A., and D. Burridge (1981), An energy and angular-momentum conserving vertical finite-difference scheme and hybrid vertical coordinates, *Mon. Weather Rev.*, *109*(4), 758–766.

Sörgel, M., et al. (2011), Quantification of the unknown HONO daytime source and its relation to NO_2, *Atmos. Chem. Phys.*, *11*, 10,433–10,447.

Szopa, S., G. Foret, L. Menut, and A. Cozic (2009), Impact of large scale circulation on European summer surface ozone and consequences for modelling forecast, *Atmos. Environ.*, *43*(6), 1189–1195.

Tang, Y., J. McQueen, S. Lu, T. Black, Z. Janjic, M. Iredell, C. Perez, and O. Jorba (2009), Recent status of NEMS/NMMB-AQ development, paper presented at 8th Annual CMAS Conference, U.S. Environ. Prot. Agency, Chapel Hill, N. C.

Vukovic, A., B. Rajkovic, and Z. Janjic (2010), Land ice sea surface model: Short description and verification, paper presented at 2010 International Congress on Environmental Modelling and Software Modelling for Environment's Sake, Int. Environ. Modell. and Software Soc., Ottawa.

Wennberg, P., and D. Dabdub (2008), Rethinking ozone production, *Science*, *319*(5870), 1624–1625.

Wentzell, J., C. Schiller, and G. Harris (2010), Measurements of HONO during BAQA-MET, *Atmos. Chem. Phys.*, *10*, 12,285–12,293.

Wesely, M. (1989), Parameterization of surface resistances to gaseous dry deposition in regional-scale numerical models, *Atmos. Environ.*, *23*(6), 1293–1304.

Wild, O., X. Zhu, and M. Prather (2000), FAST-J: Accurate simulation of in- and below-cloud photolysis in tropospheric chemical models, *J. Atmos. Chem.*, *37*(3), 245–282.

Yarwood, G., S. Rao, M. Yocke, and G. Whitten (2005), Updates to the carbon bond chemical mechanism: Cb05, *Rep. RT-0400675*, U.S. Environ. Prot. Agency, Washington, D. C.

Zilitinkevich, S. (1965), Bulk characteristics of turbulence in the atmospheric planetary boundary layer, *Tr. GGO*, *167*, 49–52.